Role of Solvent Trapping Effects in Determining the Structure and Morphology of Ternary Blend Organic Devices

Kerry B. Burke,[†,‡] Warwick J. Belcher,[†] Lars Thomsen,[†,§] Benjamin Watts,*[,||,#] Christopher R. McNeill,[⊥] Harald Ade,[||] and Paul C. Dastoor*[,†]

Centre for Organic Electronics, University of Newcastle, Callaghan, NSW 2308, Australia, CSIRO Energy Centre, Mayfield West, NSW 2304, Australia, Australian Synchrotron Company Ltd., Clayton, Vic 3168, Australia, Department of Physics, North Carolina State University, Raleigh, North Carolina 27695, and Cavendish Laboratory, J. J. Thomson Avenue, Cambridge CB3 0HE, United Kingdom,

Received November 24, 2008; Revised Manuscript Received February 22, 2009

ABSTRACT: We present results of scanning transmission X-ray microscopy (STXM) measurements of bulk heterojunction organic solar cells built from a ternary blend of poly(3-hexylthiophene) (P3HT), [6,6]-phenyl-C61-butyric acid methyl ester (PCBM), and [2,3,12,13-tetracyano-5,10,15,20-tetrakis(3,5-di-*tert*-butylphenyl)porphyrinato]copper(II) ($Cu(CN)_4P$) porphyrin. These results show evidence of solvent trapping due to porphyrin in the film. Upon annealing, submicrometer depressions are observed in the ternary blend films, corresponding to the evolution of solvent that is associated with the small porphyrin aggregates that phase segregate in the middle of the depressions. The areal density and size of the depressions change systematically with porphyrin concentration in the ternary blend. The relationship of the observed morphologies to the previously measured device performance is discussed.

Introduction

Photovoltaic devices based on blends of conjugated polymers offer the prospect of low cost renewable energy generation.[1] Indeed, solid state heterojunction devices based on binary blend structures have already demonstrated power conversion efficiencies of between 4 and 6% under AM1.5 solar irradiation. The best devices are fabricated from mixtures of poly(3-hexylthiophene) (P3HT) and [6,6]-phenyl-C61-butyric acid methyl ester (PCBM)[2] and are now commercially viable.[1] However, a key limitation to further improvement in the performance of these organic photovoltaic devices is their limited sensitivity to the longer wavelength components of the solar spectral range. In particular, the absorption of these devices, governed primarily by the band gap of the semiconducting polymer component, reduces significantly at wavelengths above about 600 nm.[3]

One way to overcome the spectral limitation involves the incorporation of additional chromophores with absorption spectra that are complementary to that of the polymer−fullerene blend. An added complexity with these ternary blend devices is that as well as acting as complementary light-harvesters, these materials must also be capable of mixing intimately in the blend structure and participating in charge transfer to and from the other components. Porphyrins are an attractive choice as this kind of additive because of their key role in photosynthesis[4] and their roles in natural systems in exciton transport and separation, and in charge transport.[4,5] Furthermore, routine synthetic modification of the porphyrin molecule allows the absorption spectrum to be tailored to further compliment that of the conducting polymer. Unfortunately, attempts to incorporate porphyrins into solid-state devices have thus-far resulted in limited success. Porphyrin-based solid-state devices, in which the porphyrin is vacuum deposited as a single film[4] or as one of two films in a p−n junction device,[6] sandwiched between metal electrodes show low efficiencies. This has been attributed to the low exciton diffusion length in the evaporated film (typically less than 10 nm). By comparison, phthalocyanines exhibit longer exciton diffusion lengths (reported to be as high as 68 nm[7]) and as a result copper phthalocyanine−C60 p−n junction devices showed considerably higher efficiencies than their porphyrin counterparts.[8] Codeposition of copper phthalocyanine (CuPc) and C60 with subsequent annealing[9] resulted in the formation of efficient two-component bulk heterojunction films showing that efficient solid-state devices incorporating porphyrins are indeed feasible. The specialized spectral response of porphyrins has also been utilized for narrow-band detection at the violet end of the visible spectrum via the formation of binary blend devices.[10,11] However, despite the perceived potential for porphyrins to be incorporated into organic photovoltaic devices there have been few reports of their successful inclusion into polymer:fullerene bulk heterojunction (BHJ) devices.

Earlier work has shown that porphyrins can be successfully incorporated into ternary blend devices containing MEH−PPV as the active polymer component, with the optimized ternary blend devices exhibiting comparable device efficiencies to the binary blend structures. Moreover, this work showed that all three components (polymer, fullerene, and porphyrin) participated significantly in light harvesting, principal charge separation and charge transport.[12] Additionally, this work showed that, contrary to general expectations in the field, the fullerene component actually plays a major role in *light harvesting* as well as in charge conduction.[12] More recently, attempts were made to incorporate the same porphyrin into polymer blend devices containing P3HT as the active component. However, in this case, the performance of the ternary blend OPV devices was much worse than that of the binary structures without porphyrin. In particular, the photocurrent generated by light absorbed by the porphyrin component was lost upon annealing the devices.[13]

* Corresponding author. Telephone: +61 2 49215426. Fax: +61 2 49216907. E-mail: phpd@alinga.newcastle.edu.au.
[†] Centre for Organic Electronics, University of Newcastle.
[‡] CSIRO Energy Centre.
[§] Australian Synchrotron Company Ltd.
[||] Department of Physics, North Carolina State University.
[#] Present address: Swiss Light Source, Paul Scherrer Institut, 5232 Villigen PSI, Switzerland.
[⊥] Cavendish Laboratory.

10.1021/ma802632y CCC: $40.75
Published on Web 03/30/2009

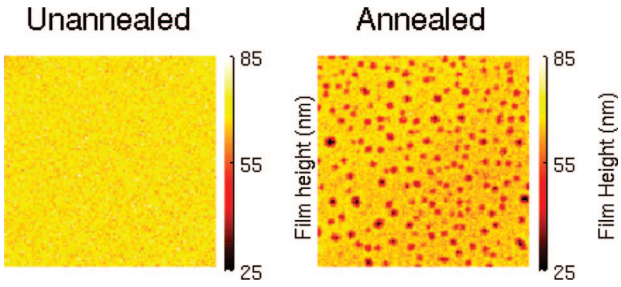

Figure 1. 20 × 20 μm STXM thickness maps of unannealed (A) and annealed (B) 1:1:1 P3HT/PCBM/porphyrin blend films.

It is well established that the morphology of polymer blends plays a key role in determining the energy conversion efficiency of bulk heterojunction devices.[14,15] It seems reasonable to speculate, therefore, that the poor performance observed in the P3HT-based ternary blend devices arises from annealing induced morphological changes. However, our previous investigations revealed no difference between annealed and unannealed films on an optical length scale.[13]

Scanning transmission X-ray microscopy (STXM) is a powerful synchrotron-based technique that probes both the structure and the composition of polymer blend films with nanoscale resolution.[19,20] Using this technique, we have reported a number of investigations detailing the relationship between film morphology and OPV device performance across a variety of binary blend systems.[16,17] In this paper we present results of STXM studies of P3HT/PCBM/porphyrin ternary blends probing the structure−function relationship in these materials and highlighting the role that solvent−porphyrin interactions play in the development of film morphology in ternary blends.

Experimental Section

Materials. P3HT was supplied by American Dye Source, Inc. (Mw 32 000 g/mol). PCBM was supplied by Solenne BV. $Cu(CN)_4P$ ([2,3,12,13-tetracyano-5,10,15,20-tetrakis(3,5-ditert-butylphenyl)porphyrinato]copper(II)) was prepared and supplied by the group of Prof. Crossley at the University of Sydney. All chemicals were used as supplied.

Sample Preparation. Polymer blend films were prepared as follows. Precleaned glass slides (1 × 1.5 cm) were prepared by sonicating initially in detergent solution, rinsing with deionized water and then sonicating in acetone before being stored in isopropanol. Solutions of the desired polymer, fullerene and porphyrin ratios were prepared by mixing the appropriate amounts of stock solutions of 20 g/L P3HT, PCBM and porphyrin in chloroform. These solutions were spin coated at 2000 rpm onto the precleaned glass slides to give films of thickness between 90 and 115 ± 10 nm. Film thicknesses were measured using a KLA-Tencor Alpha-step 500 surface profilometer. After spin-coating, the films were floated off into deionized water and then picked up onto copper TEM grids for analysis.

Techniques. STXM measurements were performed at the Advanced Light Source on beamline 5.3.2.[25] The TEM grid-mounted sample is rastered with respect to the X-ray beam in helium (0.33 atm) with the transmitted X-ray signal detected by a scintillator and a photomultiplier tube. The energy of the X-ray beam was varied between 250 and 700 eV, which covered the C, N, and O K-edges with a resolution of 100 meV or better at the C K-edge. The components maps in Figure 2 are derived by the following process. Lateral drifting between images at different energies were corrected by shifting the images laterally to achieve a maximum in the image correlation function. The NEXAFS spectra of the pristine P3HT, PCBM, and porphyrin spectra were normalized to mass by dividing by the density of the material and film thickness (measured using surface profilometry). At each pixel in the STXM image a five-point spectra was obtained and a least-squares fitting algorithm (constrained to positive solutions) was used to fit a sum of the three normalized pristine spectra to the measured blend spectra. The resulting coefficients are the masses of each of the three components present at that pixel and dividing each of the masses by the total mass gives the percentage composition of each component by mass. The total height of the film was obtained by dividing the mass of each component by its density and summing the resultant height of each component. These calculations are performed at each pixel, resulting in composition maps (by mass) and a total height map. The composition maps have been filtered with a circular Chebyshev polynomial filter. Further details of experiment and data analysis can be found elsewhere.[18] Image analysis was assisted by use of the IDL widget aXis2000 (http://unicorn.mcmaster.ca/aXis2000.html).

Results and Discussion

P3HT/PCBM/porphyrin ternary blend films were prepared in the ratios 5:5:n where n was varied from 1 to 5 in integer steps in accordance with the blend ratios reported in previous studies.[13] Figure 1 shows 20 × 20 μm images of the film thickness for an unannealed and annealed 1:1:1 blend obtained by STXM. Previous work has shown that the calculated thickness maps correlate directly with thickness measurements obtained from atomic force microscopy.[18] The unannealed film exhibits an essentially featureless morphology comparable to the morphologies observed for binary P3HT:PCBM films. Moreover, a comparable structure was observed for all unannealed blend ratios studied here. By comparison, the thickness map of the annealed 1:1:1 blend shows distinct circular depressions that are distributed uniformly across the film and which penetrate approximately two-thirds of the thickness of the film. The majority of the depressions are submicrometer in diameter with only a few of the largest features being on the order of 1 μm in diameter. Moreover, similar depressions are observed in all blend ratios with a relative porphyrin content above 5:5:1.

The observation of morphological features on the submicrometer scale could provide an explanation for the poor performance of the annealed ternary blend films. In particular, phase segregation of polymer blends on this length scale has been shown to disrupt the interpenetrating networks required for an optimal bulk heterojunction device.[18] In order to probe the relationship between morphology and composition in these films STXM compositional maps were obtained for all of the ternary blend ratios. For the unannealed blend films, uniform compositional maps (not shown) were obtained for the P3HT, PCBM and porphyrin components. Moreover, the calculated compositions agreed with the values expected from the nominal bulk blend ratios to within ±12%.

Figure 2 shows the P3HT, PCBM and porphyrin compositional maps for the annealed films with blend ratios from 5:5:1 to 5:5:5. In addition, the thickness map for each blend ratio is shown and circular depressions are observed for the annealed films with blend ratios from 5:5:2 to 5:5:5, with the thickness map for the 5:5:1 blend being essentially featureless. A comparison of the compositional maps for each of the three components with the corresponding thickness map shows some general correlations. In particular, in the regions of the circular depressions there appears to be a general enhancement of the porphyrin concentration and a corresponding reduction in both the P3HT and PCBM relative concentrations. Phase segregation is also observed on the sub micrometer scale throughout the 5:5:1 film and in the regions between the depressions in the 5:5:2 to 5:5:5 films. Thus it would appear that the formation of the circular depressions in the ternary blend film morphology is associated with porphyrin aggregation in the film. Furthermore, the fact that neither depressions nor porphyrin segregation is observed in the 5:5:1 film suggests that there is a threshold

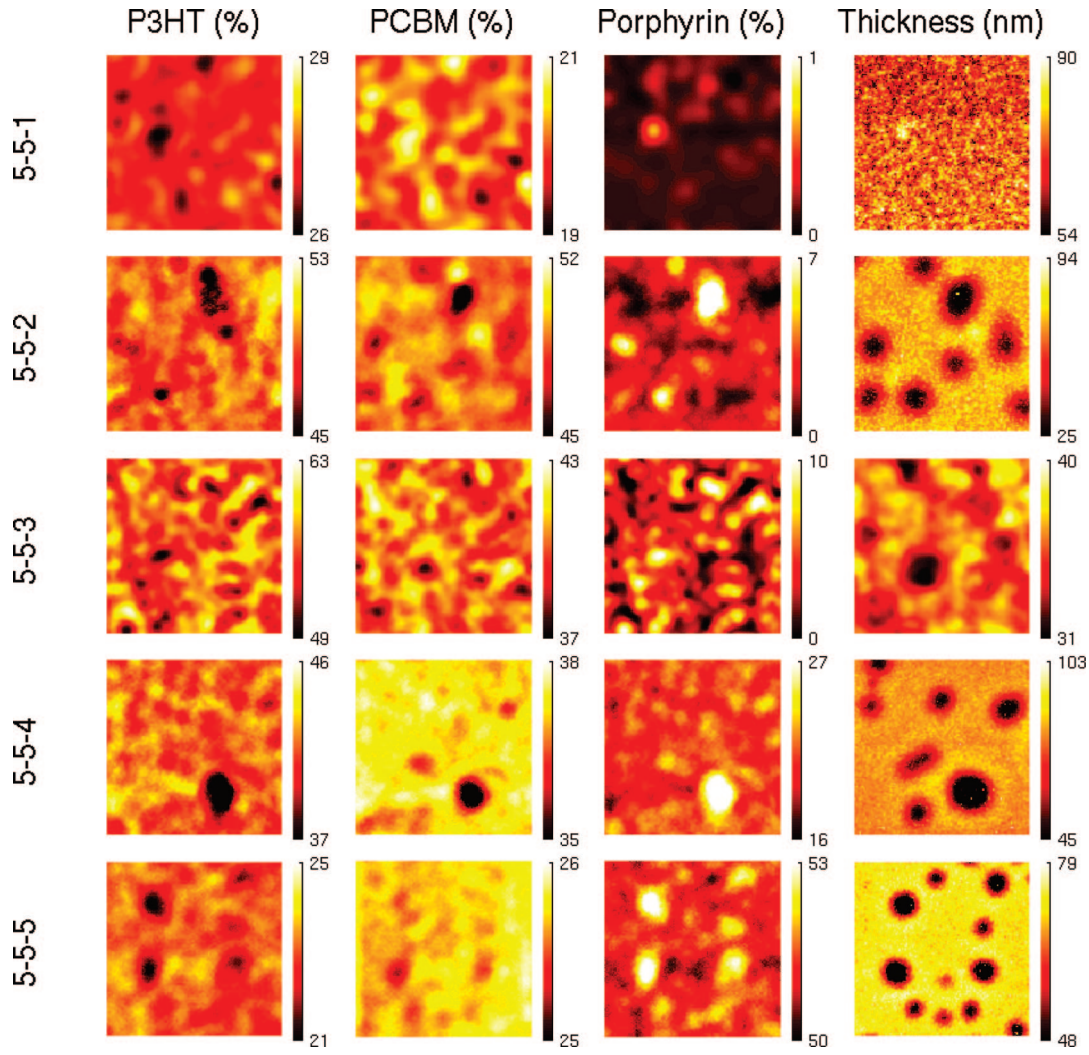

Figure 2. 5 × 5 μm compositional maps of P3HT, PCBM, and porphyrin concentration for blend ratios 5:5:1 to 5:5:5 together with the corresponding thickness maps.

porphyrin concentration required for formation of these structures.

The profile of the thickness and porphyrin concentration for a typical depression is shown in Figure 3. The profiles were obtained by rotationally averaging about the center of the depression.[21] The center of the depression is approximately one-third of the thickness of the surrounding film, and a distinct ridge or lip can be observed at the edge of the depression approximately 750 nm from the center of the feature. The porphyrin concentration is at a maximum in the center of the depression and shows an approximate 100% enhancement over the bulk film value.

This profile can be explained in terms of the aggregation properties of porphyrins. Porphyrins are well-known to aggregate via π-stacking of the porphyrin rings, both in solution and in the solid-state.[22] These aggregates form body centered cubic structures which act as clathrates and as such can readily incorporate small moieties such as solvent molecules.[23] The typical host−guest molecule ratio is between 1:2 and 2:1, with the vast majority adopting the former ratio.[23] Thus, we propose that following spin-coating of ternary porphyrin blends, solvent can either exist as residual solvent within the bulk of the film or specifically entrapped within porphyrin clathrates. Annealing, which involves heating the film above its glass transition point, facilitates mobility of the components and associated solvent resulting in the observed aggregation of the porphyrin clathrates. The absence of any depressions within the binary blend films

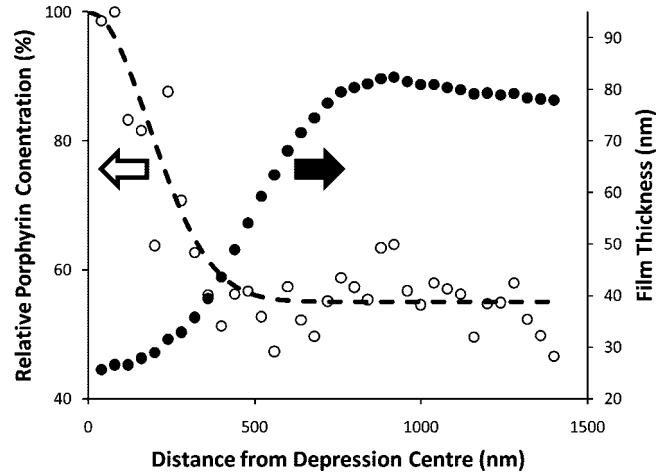

Figure 3. Variation of average film thickness and porphyrin concentration (relative to the porphyrin concentration at the center of the depression) as a function of distance across a typical circular depression in the 5:5:4 blend film. The dashed line has been added to the concentration profile as a guide to the eye.

suggests that residual solvent is readily released during the annealing process via diffusion without causing any structural changes to the film. In contrast, clathrates release bound solvent via a thermally activated desorption process characterized by a

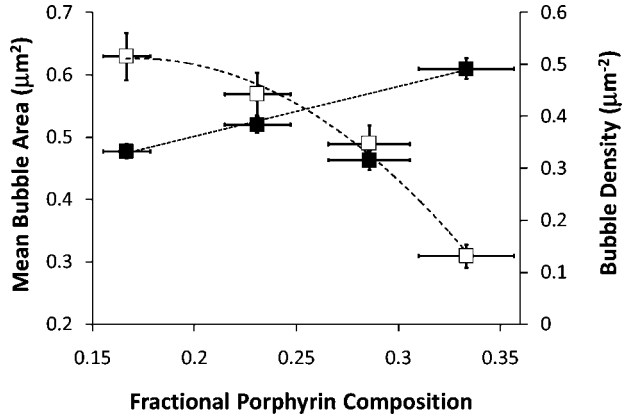

Figure 4. Variation of mean bubble area and density with fractional porphyrin concentration. The dashed lines have been added as a guide for the eye.

sharp transition temperature above that of the boiling point of the pure solvent.[24] It seems reasonable to hypothesize therefore that the porphyrin aggregates act as point sources for solvent evolution during the annealing process producing a gas bubble that subsequently collapses resulting in the observed depressions in the film. Moreover, the presence of a raised rim around the depression is consistent with the deposition of debris associated with the sudden rupture of the gas bubble. Thus the model picture is one of a gas bubble that bursts rather than deflates slowly in time.

The evolution of a solvent bubble results in deformation of the surrounding matrix (Figure 3) and the maximum deformation that the film can withstand before the bubble collapses and evolves gas depends upon the tensile strength of the film. For a given blend composition the tensile strength of the film is fixed resulting in a relatively constant bubble size as observed in Figure 2. Furthermore, increasing the porphyrin concentration in the ternary blend lowers its fractional polymer content and hence the tensile strength of the film since the polymer is the main film-forming component. Therefore, the maximum deformation that the film can withstand is reduced, resulting in smaller bubbles.

The mean bubble size and density were extracted from each STXM image by using an image analysis algorithm that determined the number of features in the total thickness maps that possessed a contrast below a certain filter threshold level. Figure 4 shows that there is indeed a clear trend toward smaller bubble size, with a corresponding increase in bubble density, with increasing fractional porphyrin as expected, thus providing further support for the solvent evolution model described above.

Further support for the hypothesis that the observed bubbles are a consequence of the evolution of entrapped solvent is provided by a calculation of the solvent to porphyrin molar ratio. Figure 5 shows the key parameters used in this calculation. Assuming cylindrical symmetry, the number of moles of porphyrin between r and $r + \delta r$ from the center of the depression is given by:

$$dm_{\mathrm{por}} \approx \frac{2\pi r \rho h(r) f(r) \delta r}{M_{por}} \tag{1}$$

Here, ρ is the density of the porphyrin, M_{por} is the molecular weight of the porphyrin, $h(r)$ is the film thickness profile and $f(r)$ is the fractional concentration profile of the porphyrin.

The corresponding number of moles of solvent between r and $r + \delta r$ from the center of the depression assuming a hemispherical bubble height profile of radius, r_c is given by

$$dm_{\mathrm{solv}} \approx \frac{2\pi r(h_{\mathrm{m}} - h(r) + h_{\mathrm{b}})\delta r}{V_{\mathrm{m}}} = \frac{2\pi r(h_{\mathrm{m}} - h(r) + \sqrt{r_{\mathrm{c}}^2 - r^2})\delta r}{V_{\mathrm{m}}} \tag{2}$$

where V_{m} is the molar volume, h_{m} is the maximum film thickness and $h_{\mathrm{b}}(r)$ is the height of the bubble at radius r. The total number of moles solvent (or porphyrin) is obtained by summing all of the elements dm_{solv} (or dm_{por}) from $0 \le r \le r_{\mathrm{c}}$ and thus the solvent to porphyrin molar ratio is given by:

$$\frac{m_{\mathrm{solv}}}{m_{\mathrm{por}}} = \frac{M_{\mathrm{por}}}{\rho V_{\mathrm{m}}} \frac{\sum_{r=0}^{r=r_{\mathrm{c}}} r(h_{\mathrm{m}} - h(r) + \sqrt{r_{\mathrm{c}}^2 - r^2})}{\sum_{r=0}^{r=r_{\mathrm{c}}} rh(r)f(r)} \tag{3}$$

From eq 3, the solvent to porphyrin molar ratio was calculated to be 3:2 by numerically summing the data in Figure 3 and using values of $M_{\mathrm{por}} = 1205$ g mol^{-1}, $r = 1.3$ g cm^{-3}, and $V_{\mathrm{m}} = 24000$ cm mol^{-1}. Thus, the host:guest ratio calculated using this model is 2:3 and lies almost ideally within the typical range of 1:2 to 2:1 outlined previously for clathrate structures.[22] As such, this simple quantitative model provides additional support for the hypothesis that the observed depressions are associated with evolved solvent associated with the porphyrin content of the film.

There are a number of other possible mechanisms that could potentially account for the formation of the observed depressions. The depressions could be the result of the evolution of residual solvent from within the bulk film. In this case, the porphyrin aggregates would act as nucleation centers for bubble formation rather than as point sources of entrapped solvent. However, this mechanism seems unlikely since it is known that PCBM forms similar aggregates upon annealing within binary P3HT:PCBM films and yet depressions are not observed in these annealed films.[15]

Alternatively, the observed depressions could arise from a dewetting process between the polymer blend and the substrate. In this case, at temperatures above the glass transition temperature of the blend, dewetting of the substrate by the polymer matrix could occur around the porphyrin aggregates. This process could result in the formation of circular "voids" around the porphyrin crystallites within the film and in the evolution of solvent trapped in the film as a gas bubble. In the absence of a polymer matrix, Liu et al. have reported a similar mechanism for the formation of gas bubbles during the evaporation of chloroform solutions of porphyrin and observed that nucleation around a foreign particle (corresponding here to the porphyrin aggregate) reduced the free energy barrier for bubble formation.[26] Again, it seems probable that this process can be

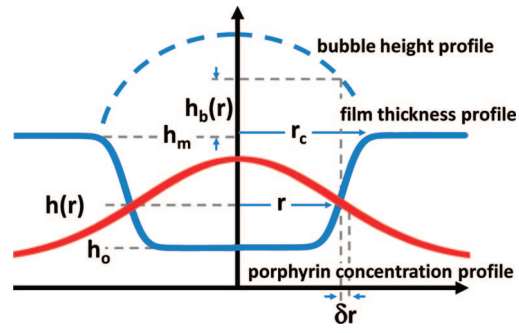

Figure 5. Schematic diagram illustrating the key parameters in the solvent evolution model.

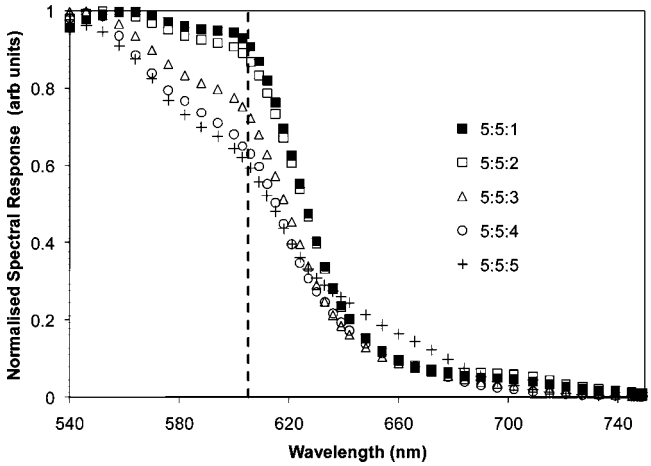

Figure 6. Normalized spectral response as a function of porphyrin composition for blend ratios 5:5:1 to 5:5:5. The vertical dashed line is at 604 nm and marks the position of the P3HT vibronic peak that is a signature of improved polymer ordering.

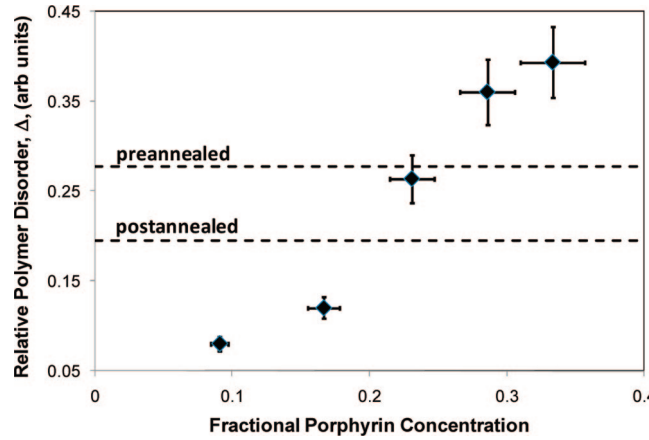

Figure 7. Variation of the polymer disorder parameter (Δ) as a function of porphyrin concentration for ternary blend ratios 5:5:1 to 5:5:5. The upper and lower horizontal dashed lines show the value of the disorder parameter for preannealed and postannealed P3HT:PCBM binary blend devices, respectively.

discounted since dewetting is not observed for the binary P3HT:PCBM systems.

Finally, the depressions could be due to material depletion from the bulk film during the formation of porphyrin aggregates via phase segregation. In other words, the formation of porphyrin aggregates during annealing results in depletion of porphyrin from the surrounding film with an associated thinning of the film. Similar effects are observed as a result of the formation of PCBM crystallites during annealing in binary blends[16,28] and also in nonpolymer based binary systems.[27] However, conservation of mass considerations would mean that in this mechanism a raised crystallite of porphyrin would be observed at the center of the depression. While for the ternary blends films the porphyrin concentration is enhanced at the center of the depression, no raised region is observed. Moreover, there is still considerable porphyrin concentration present within the bulk of the film surrounding the depression, suggesting that the main driver for the formation of the depressions is not demixing of the porphyrin from the other two components.

Thus, in the light of the preceding discussion, we believe that the observed depressions arise from the evolution of solvent trapped within porphyrin clathrates within the film. It is clear therefore that the formation of these depressions is associated with considerable changes in the morphology of the blend film and, as such, might be expected to have a significant impact upon the performance of photovoltaic devices built from these ternary blend structures.

Previous work on the device characteristics of these ternary blend devices revealed significant differences between the spectral response of the unannealed and annealed blends.[13] For the unannealed films, the addition of porphyrin resulted in a dramatic reduction in the polymer contribution to the photocurrent response and the observation of a relatively strong porphyrin response in the devices. Upon annealing a reduction of the porphyrin response in the devices was observed together with some recovery of the P3HT response.[13]

It is well established that the wavelength dependent absorption behavior (and hence spectral response) of P3HT blend devices reflect the crystallinity of the polymer domains.[29] In particular, the presence of vibronic structure at 604 nm corresponds to a structuring of the P3HT chains.[30] For binary blends, this peak is reduced upon the addition of PCBM and is restored upon annealing.[31]

Figure 6 shows the variation of spectral response (normalized to the maximum response) for the postannealed devices as a function of porphyrin concentration for blend ratios 5:5:1 to 5:5:5. There is a systematic decrease in the relative height of the vibronic peak at 604 nm with increasing porphyrin concentration suggesting that the degree of disorder of the polymer domains also systematically increases. In order to quantify this behavior further, we have defined a relative polymer disorder parameter, Δ, in terms of the difference between the normalized intensity of the vibronic peak relative to the maximum intensity, thus:

$$\Delta = \frac{(I_{\max} - I_{604})}{I_{\max}} \tag{4}$$

Figure 7 shows that, as expected, the polymer disorder parameter increases systematically with increasing porphyrin concentration and appears to approach an asymptotic limit for the 5:5:5 ternary blend device. Interestingly, for the 5:5:1 and 5:5:2 ternary devices, the degree of polymer disorder is actually less than that observed in both the pre- and postannealed binary blend devices.

Combining these observations together allows us to develop a consistent picture of the role of structure and morphology in determining the performance of P3HT:PCBM:porphyrin ternary blend devices. Our previous work showed that, upon annealing, no photocurrent was generated by the porphyrin component of the ternary blend; suggesting that phase segregation occurs at all blend ratios.[13] Moreover, at low porphyrin concentrations, the addition of porphyrin improves the organization of the P3HT chains upon annealing. Similar behavior has been observed upon the addition of carbon nanotubes to P3HT:PCBM binary blends and suggests that, upon annealing, there is a reduced association of the porphyrin and PCBM components with the P3HT chains resulting in increased polymer order but a reduced ability for charges generated by light absorbed by the porphyrin to be transported to the electrodes.[32] As the porphyrin concentration is increased, then bubble formation is observed with increasing density in the postannealed ternary blend films. These bubbles are formed from entrapped solvent in the film associated with porphyrin aggregates that act as clathrates and the size of these bubbles is consistent with the expected host:guest ratios expected for such structures. Polymer disorder increases systematically with increasing bubble density, with the increasing disruption of the P3HT chains hindering charge transport and device performance. In general, the typical size of the bubbles is below the resolution limit of most optical microscopy and was only revealed by the much lower resolution limit of the STXM technique. The results presented here demonstrate the impor-

tance of solvent interactions in polymer blend films and their impact upon submicrometer structure and morphology and hence device performance. Although these interactions are particularly enhanced for the porphyrin ternary blend structures presented here, they are also likely to be relevant to many other electronic polymer blend systems.

Conclusions

The device performance of ternary blend P3HT:PCBM:porphyrin devices is strongly influenced by the resulting morphology of the blend film. The morphology of films with porphyrin blend ratios from 5:5:2 to 5:5:5 appears to be determined in part by solvent−porphyrin interactions with solvent entrained within porphyrin aggregates in the film. Upon annealing this entrapped solvent is released producing submicrometer depressions throughout the film. With increasing porphyrin concentration there is a corresponding increase in both the observed density of these depressions and the degree of disorder in the P3HT component of the film. The observed changes in morphology are consistent with the photovoltaic performance of the ternary blend devices, which also show that the disorder of the P3HT polymer chains increases with increasing bubble density. The results presented here reveal that solvent entrapment has a significant effect upon the submicrometer morphology of ternary blend films and that new fabrication strategies need to be developed to eliminate these solvent-based effects.

Acknowledgment. The authors thank the ALS for beamtime and David Kilcoyne for technical assistance. Professor Crossley and colleagues at the University of Sydney are gratefully acknowledged for the porphyrin synthesis. This work was supported by the Engineering and Physical Sciences Research Council, U.K. (SUPERGEN IV) and by the Australian Research Council's Discovery funding scheme (DP0559417). We acknowledge financial support from the Commonwealth of Australia through the Access to Major Research Facilities Program. The ALS is supported by the Director, Office of Science, Office of Basic Energy Sciences, of the U.S. Department of Energy under Contract No. DE-AC02-05CH11231. B. Watts and H. Ade supported by US Department of Energy under Grant DE-FG02-98ER45737.

References and Notes

(1) Brabec, C. J.; Durrant, J. R. *MRS Bull.* **2008**, *33*, 670.
(2) Kim, J.; Kim, S.; Lee, H.; Lee, K.; Ma, W.; Huong, X.; Heeger, A. *J. Adv. Mater.* **2006**, *18*, 572.
(3) Günes, S.; Neugebauer, H.; Sariciftci, N. S. *Chem. Rev.* **2007**, *107*, 1324.
(4) Tang, C. W.; Albrecht, A. C. *Nature* **1975**, *254*, 507.
(5) Deisenhofer, J., Norris, J. R., Eds. *The Photosynthetic Reaction Center*; Academic Press: San Diego, CA, 1993.
(6) Günster, S.; Siebentritt, S.; Elbe, J.; Kreienhoop, L.; Tennigkeit, B.; Wöhrle, D.; Memming, R.; Meissner, D. *Mol. Cryst. Liq. Cryst.* **1992**, *218*, 117.
(7) Stubinger, T.; Brütting, W. J. *Appl. Phys.* **2001**, *90*, 3232.
(8) Peumans, P.; Forrest, S. R. *Appl. Phys. Lett.* **2001**, *79*, 126.
(9) Peumans, P.; Uchida, S.; Forrest, S. R. *Nature* **2003**, *425*, 158.
(10) Takahashi, K.; Asano, M.; Imoto, K.; Yamaguchi, T.; Komura, T.; Nakamura, J.; Murata, K. J. *Phys. Chem. B* **2003**, *107*, 1646.
(11) Takahashi, K.; Nakajima, I.; Imoto, K.; Yamaguchi, T.; Komura, T.; Murata, K. *Sol. Energy Mater. Sol. Cells* **2003**, *76*, 115.
(12) Dastoor, P. C.; McNeill, C. R.; Frohne, H.; Foster, C. J.; Dean, B.; Belcher, W. J.; Fell, C. J.; Campbell, W. M.; Officer, D. L.; Blake, I. M.; Thordarson, P.; Crossley, M. J.; Hush, N. S.; Reimers, J. R. *J. Phys. Chem. C* **2007**, *111*, 15415.
(13) Belcher, W. J.; Wagner, K. I.; Dastoor, P. C. *Sol. Energy Mater. Sol. Cells* **2007**, *91* (6), 447.
(14) Hoppe, H.; Niggemann, M.; Winder, C.; Kraut, J.; Hiesgen, R.; Hinsch, A.; Meissner, D.; Sariciftci, N. S. *Adv. Funct. Mater.* **2004**, *14*, 1005.
(15) McNeill, C. R.; Watts, B.; Thomsen, L.; Belcher, W. J.; Kilcoyne, A. L. D.; Greenham, N. C.; Dastoor, P. C. *Small* **2006**, *2*, 1432.
(16) McNeill, C. R.; Frohne, H.; Holdsworth, J. L.; Furst, J. E.; King, B. V.; Dastoor, P. C. *Nano Lett.* **2004**, *4*, 219.
(17) McNeill, C. R.; Frohne, H.; Holdsworth, J. L.; Dastoor, P. C. *Nano Lett.* **2004**, *4*, 2503.
(18) McNeill, C. R.; Watts, B.; Thomsen, L.; Belcher, W. J.; Greenham, N. C.; Dastoor, P. C. *Nano Lett.* **2006**, *6*, 1202.
(19) Ade, H.; Zhang, X.; Cameron, S.; Costello, C.; Kirz, J.; Williams, S. *Science* **1992**, *258*, 972.
(20) Ade, H.; Hitchcock, A. P. *Polymer* **2008**, *49*, 643.
(21) Fujita, T.; Chen, M. W. *Jpn. J. Appl. Phys.* **2008**, *47*, 1161.
(22) Elwmans, J. A. A. W.; van Hameren, R.; Nolte, R. J. M.; Rowan, A. E. *Adv. Mater.* **2006**, *18*, 1251.
(23) Byrn, M. P.; Curtis, C. J.; Hsiou, Y.; Khan, S. I.; Sawin, P. A.; Tendick, S. K.; Terzis, A.; Strouse, C. E. *J. Am. Chem. Soc.* **1993**, *115*, 9480.
(24) Pekker, S.; Faigel, G.; Fodor-Csorba, K.; Gránásy, L.; Jakab, E.; Tegze, M. *Solid State Commun.* **1992**, *83*, 423.
(25) Kilcoyne, A. L. D.; Tyliszczak, T.; Steele, W. F.; Fakra, S.; Hitchcock, P.; Franck, K.; Anderson, E. H.; Harteneck, B. D.; Rightor, E. G.; Mitchell, G. E.; Hitchcock, A. P.; Yang, L.; Warwick, T.; Ade, H. *J. Synchrotron Radiat.* **2003**, *10*, 125.
(26) Schenning, A. P. H. J.; Benneker, F. B. G.; Geurts, H. P. M.; Liu, X. Y.; Nolte, R. J. M. *J. Am. Chem. Soc.* **1996**, *118*, 8549.
(27) Savenije, T. J.; Kraoeze, J. E.; Yang, X.; Loos, J. *Adv. Funct. Mater.* **2005**, *15*, 1260.
(28) Denker, U.; Schmidt, O. G.; Jin-Philipp, N.-Y.; Eberl, K. *Appl. Phys. Lett.* **2001**, *78*, 3723.
(29) Kim, Y.; Choulis, S. A.; Nelson, J.; Bradley, D. D. C.; Cook, S.; Durrant, J. R. *J. Mater. Sci.* **2005**, *40*, 1371.
(30) Ikeda, A.; Nobusawa, K.; Hamano, T.; Kikuchi, J. *Org. Lett.* **2006**, *8*, 5489.
(31) Erb, T.; Zhokhavets, U.; Gobsch, G.; Raleva, S.; Stuhn, B.; Schilinsky, P.; Waldauf, C.; Brabec, C. J. *Adv. Funct. Mater* **2005**, *15*, 1193.
(32) Berson, S.; de Bettignies, R.; Bailly, S.; Guillerez, S.; Jousselme, B. *Adv. Funct. Mater* **2007**, *17*, 3363.

MA802632Y